Pergamon

International Journal of Machine Tools & Manufacture 40 (2000) 739–768

INTERNATIONAL JOURNAL OF
MACHINE TOOLS
& MANUFACTURE
DESIGN, RESEARCH AND APPLICATION

On-line metal cutting tool condition monitoring. I: force and vibration analyses

D.E. Dimla Sr. [a,*], P.M. Lister [b]

[a] *School of Mechanical and Offshore Engineering, The Robert Gordon University, Schoolhill, Aberdeen AB10 1FR, UK*

[b] *School of Engineering and the Built Environment, The University of Wolverhampton, Wulfruna St, Wolverhampton WV1 1SB, UK*

Received 26 March 1999; accepted 27 September 1999

Abstract

Excessive wear on cutting tools give rise to distortions in dimension of manufactured components, sometimes increasing scrapped levels thereby incurring additional costs. Methods for detecting and monitoring the wear on a cutting tool is therefore crucial in most metal cutting processes and several research efforts have striven to develop on-line tool condition monitoring systems. This paper describes an experimental and analytical method for one such technique involving the use of three mutually perpendicular components of the cutting forces (static and dynamic) and vibration signature measurements. The ensuing analyses in time and frequency domains showed some components of the measured signals to correlate well to the accrued tool wear. © 2000 Elsevier Science Ltd. All rights reserved.

Keywords: Static force; Dynamic force; Vibration signature; Time series and frequency analyses; Tool wear; Metal turning; Chip breaker

1. Introduction

The last three decades has witnessed the launch of a technical revolution in manufacturing industries, the installation of automated robots and computers. It was initially predicted that these innovative devices would make the jobs of humans much easier, but in effect it turned out to be taking their jobs altogether. The tremendous drive towards cost savings and productivity improvements as well has led to an unabated industrial expansion through a reduction of manned processes

* Corresponding author.
E-mail address: d.dimla@rgu.ac.uk (D.E. Dimla Sr.)

0890-6955/00/$ - see front matter © 2000 Elsevier Science Ltd. All rights reserved.
PII: S0890-6955(99)00084-X

and a shrinking workforce signalling the end of the jobs-for-life ethics. However, not all-industrial activities have been automated. In metal cutting operations one of the major obstacles to realising its complete automation is that of the cutting tool-state prediction, where tool-wear is an important factor in productivity and manufacturing efficiency. In machining processes, the automation of tool-wear monitoring inevitably involve the integration of sensors in production machines and the processing and analysis of the signals with the goal of increasing productivity, reliability and quality. Implementation of a well-guided tool condition monitoring system (TCMS) is paramount to machining operations whose environment changes unpredictably. Accomplishment of such a system requires a sensor mechanism that can closely replicate the operations of the human operator whose pace and cost might be considered inadequate in the machining environment [1]. Such a system, one believes would reduce labour costs and downtime, meanwhile provide a damage limitation system for the machine tool. The realisation of total automation in metal cutting operations requires continuous monitoring to check the tool-state and dimensional integrity of the workpiece. The seemingly paradoxical combination of randomness and structure in the cutting tool-workpiece interface makes prediction of the cutting tool-state rather difficult.

Metal cutting broadly constitutes turning, boring, drilling, facing, forming and parting-off, milling and shaping/planning. Cutting tools generally can be classed into two categories: single point tools (turning, shaping, planning) which have one cutting part and a shank, while multiple tool points (drilling, milling, broaching) have more than one cutting parts. Fig. 1 shows the most commonly used terms and tool geometry definition of a typical metal cutting tooling system.

This study mainly focuses on turning, which could be defined as a machining process for generating external surfaces by the action of a cutting tool on a rotating workpiece, usually carried out on a lathe. Two kinds of metal cutting operations in turning can be encountered; oblique and orthogonal cutting.

Orthogonal cutting, could be argued, represents a reasonable approximation of cutting on the

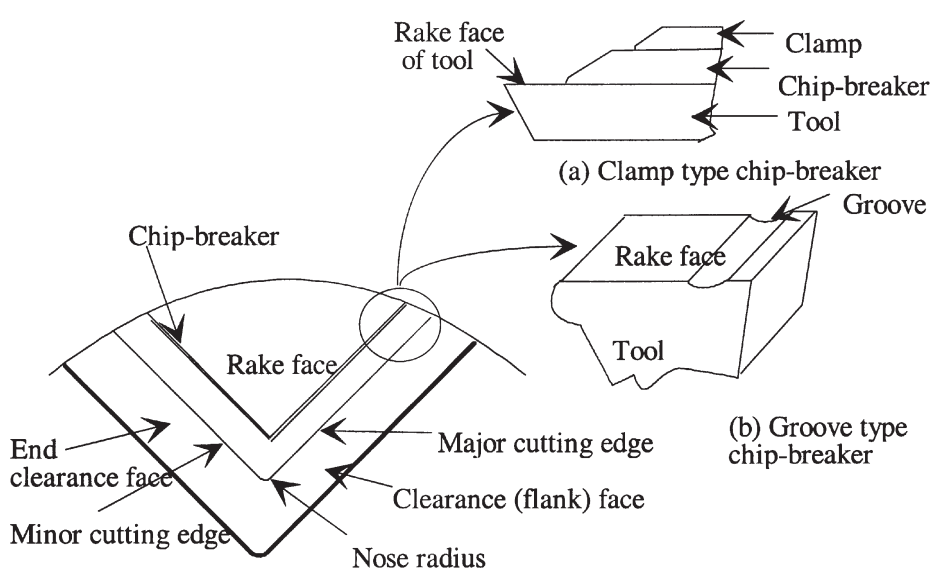

Fig. 1. Cutting tool terminology.

major cutting edges and therefore is the most prevalent form of cutting [2]. In orthogonal cutting the cutting tool approaches the workpiece at right angles to the direction of cutting, with the cutting edge parallel to the uncut surface. A full understanding of the mechanics of the orthogonal cutting process is not intended to be discussed in this paper. It is, however, fair to assume that high stresses and strain rates develop as the cutting tool ploughs through the workpiece giving rise to complicated forces, high temperatures and dynamic behaviour across a broad spectrum of frequencies. Possible explanations for the increased dynamic behaviour have been put forward by Piispenen, Merchant and Zlatin, and Drucker [2]. The resulting cutting force (likewise the vibration, torque and momements) can be resolved into the tangential (vertical or *z*-axis), feed (axial or *x*-axis) and normal (thrust or *y*-axis) components (Fig. 2).

Cutting tool wear can be classified into several types as follows:

1. adhesive wear associated with shear plane deformation,
2. abrasive wear resulting from hard particles cutting action,
3. diffusion wear occurring at high temperatures, and
4. fracture wear such as chipping due to fatigue.

Tool wear processes generally occur in combination with the predominant wear mode, dependent upon the cutting conditions, workpiece tooling material and the tool insert geometry. The more predominantly occurring forms of cutting tool wear often identified as the principal types of tool wear in metal turning using single-point tools are nose, flank, notch and crater wear and Fig. 3 shows how these wear features are usually measured.

2. Monitoring tool wear

Techniques for on-line wear monitoring can be grouped into two main categories: direct sensing and indirect sensing techniques. While direct methods of wear measurement have been attempted

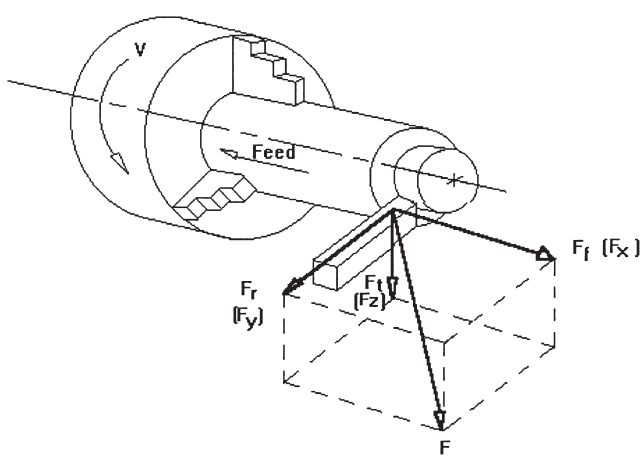

Fig. 2. Forces acting on a cutting tool in orthogonal metal cutting.

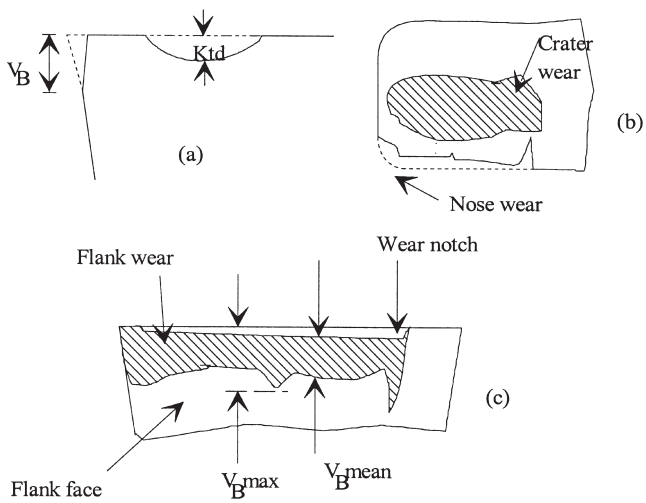

Fig. 3. Conventional features of tool wear measurements.

[1,3], the majority of methods have been indirect [1,3–11]. Direct methods are less beneficial because the cutting area is largely inaccessible, and therefore on-line monitoring can not be carried out while the tool is engaged in in-process cutting.

These methods include, amongst others, touch trigger probes, optical, radioactive, proximity sensors and electrical resistance measurement techniques [3,8,12]. Indirect methods take measurements while the tool is actively engaged, since it involves recording a variable that can be correlated to tool wear (i.e. indirect methods measure factors that result as a consequence of tool wear). Commonly used methods include amongst others cutting forces, acoustic emission, temperature, vibration, spindle motor current, torque and strain. These factors reflect far more than tool wear alone and parameters associated with tool wear must therefore be extracted from them and correlated to give a measure or extent of tool wear. The main practical drawback with this popular method is the need for calibration of the associated parameters in monitoring the cutting process. The cutting conditions (speed, feed-rate and depth of cut) are known to affect the sensor signals and a range of methods have been suggested for separating the effects of these conditions from those of wear on the measured parameter [13].

Methods for correlating the measured process parameters to tool wear, breakage or chipping fall primarily into three categories [14]. The first class consists of methods that can be viewed as heuristic based rules with a priori knowledge only of the process parameters, such as mathematical modelling and adaptive observers. The second category of methods are those that require formal knowledge of the process and can be grouped together as analytical based models such as time series analyses and Fast Fourier Transform (FFT) peak tracking. The last category is one of example based models with inductive learning capabilities such as pattern recognition, decision surfaces, mapping techniques, clustering and artificial intelligence models (neural networks, genetic algorithms and knowledge based systems).

3. Practical methods for detecting tool wear

Most indirectly measured sensor signals are generally affected by workpiece material variation, geometry and material of the cutting tool and the cutting conditions [15]. An on-line monitoring system designed to take all the aforementioned factors into consideration would be extremely demanding. In many cases, the machining system does not need to have a global knowledge of the machining process as it only requires knowledge about the machining operation in the neighbourhood of the optimum for the operating process [16]. The cutting conditions cannot be neglected, as their variable parameters affect the sensor signals and therefore the cutting tool-state. The use of indirect methods require accurate predictive models that link the un-measurable parameter of interest (tool wear), with the indirectly detectable variables [17]. The process of tapping useful signals or process parameters directly or indirectly from a cutting process constitutes what Burke [18] symbolically terms, the detection level. This level in any TCMS development is primarily concerned with choosing the relevant sensory signal.

The main objective of this study was to develop a TCMS based on analytical modelling of on-line sensor signals. Three components of cutting forces and vibration data are investigated as to their suitability for tool wear monitoring through time series and FFT analyses. The identification of signal components of the cutting process parameters that might be considered appropriate in the detection and monitoring of tool-wear was carried out from data obtained from a series of experimental test cuts. It was concluded based on the signal analyses that the chosen signals correlated well to the cutting tool wear.

4. Instrumentation and data acquisition

A test bed to generate cutting data using a variable speed centre lathe was set-up. The sensors for the vibrations and cutting forces were:

- Kistler mini accelerometers (type 8730A) for acceleration signal measurement in three mutually perpendicular directions and
- Kistler tool post dynamometer platform (type 9263A) for cutting force measurement again in three planes.

The recording instrumentation for the test bed comprised a 386 processor, 60 MHz clock speed personal computer fitted with an amplicon PC-30 data acquisition card running Windows 3.1. The signals from the sensors were passed through a signal conditioning unit and various peripheral signal conditioning instruments as shown in the schematic diagram (Fig. 4).

The two tool inserts used, P15 and P25, were cemented carbide coated via chemical vapour deposition and consisted of grades of “throw-away” indexable inserts with an integral chip-breaker geometry, held in place by a negative rake tool holder. P15 had a thick wear resistant coating on a hard resistant substrate. The inner coating was of 8 μm thickness comprising 6 μm thick of aluminium oxide (Al_2O_3) on top. The outer layer was thinner and of titanium nitride (TiN). This combination gives P15 excellent wear resistant properties. On the other hand, P25 had a thick ($\approx$10 μm) layer of Al_2O_3 on top of a medium size titanium carbon nitride (TiCN) giving it a

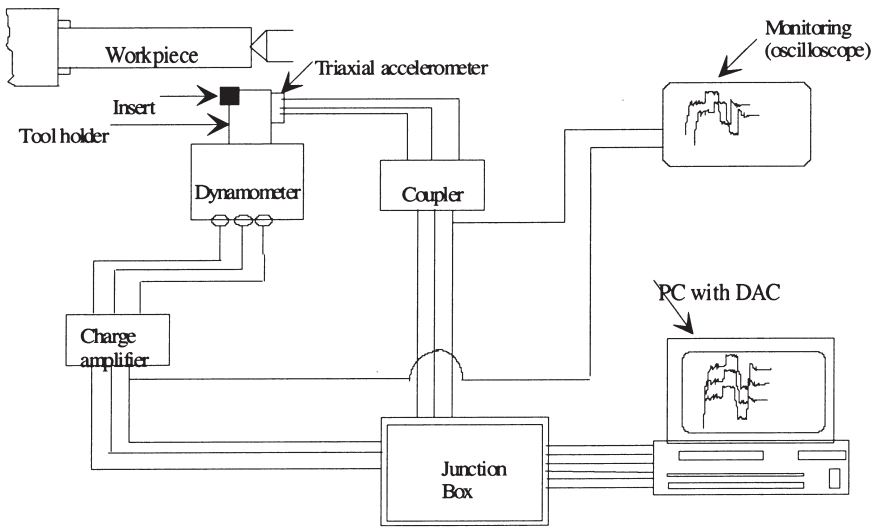

Fig. 4. The experimental test rig.

high wear resistance and good edge security [19]. No cutting fluid was used and further details of the cutting conditions are shown in Table 1. The workpiece material used was low carbon alloy steel of the EN24 type (oil quenched, rolled and tempered) which is relatively hard in order to accelerate tool-wear at the expense of a shorter tool life.

The type of metal cutting carried out was semi-orthogonal turning on a lathe as it is the most common and versatile form of metal cutting process. Like any other metal removal equipment, the ultimate economic performance of a lathe depends on the cutting tool that actually takes the chips off the workpiece. Economy and productivity have made indexable inserts the primary tooling method for lathes. With due consideration to the power limitations of the cutting machine and the particular tool/workpiece combination, the tool manufacturers specifically recommend cuts be carried within the following ranges (minimum–maximum) for each cutting parameter to incorporate various tool wear modes [19]:

Table 1
Test material type and tool details

Machine tool		Lang Swing J6
Workpiece material		
	Work material	EN24 BS 970
	Hardness	Brinell 255
	Composition	0.4% C, 0.28% Si, 0.27% Mo, 1.18% Cr, 0.5% Mn, 1.4% Ni
Tooling material		
	Tool holder	Sandvik SSBCR 2020 K12
	Tool type	SCMT 12 04 08 UM
	Tool material	Sandvik Coromant P25 4025 And P15 4015
	Overhang (mm)	45
Cutting fluid used	None	

feed-rate: 0.1–0.4 mm/rev
cutting speed: 80–350 m/min
depth of cut: 0.5–4 mm.

The selection of these parameters for any particular turning operation require a complex assortment of considerations involving the interaction of the workpiece, machine tool and tooling material as a system [20].

5. Range of cutting conditions investigated

Using the tool insert manufacturer's guidelines, a cutting range was selected based on the insert type and the ensuing cutting parameters chosen accordingly. This involved reading the maximum and minimum values of the feed-rate and depth of cut (DOC) values off ISO charts that corresponded to the chosen tool inserts. For the tools selected, the recommended values were as follows: feed-rates, 0.05–0.4 mm/rev while DOC varied from 0.2 to 4 mm. Cutting speed was selected based on the toughness of the workpiece to be machined. The recommended cutting conditions for the workpiece-tooling geometry configuration was as follows: feed-rate of 0.25 mm/rev; DOC of 1.25 mm, and cutting speed of 273 m/min.

A decision was made to conduct the wear tests at a fixed DOC of 2 mm (since DOC increments resulted only in a proportional increase in the magnitude of the process parameters) within the following conditions (though not exhaustively):

- cutting speeds: 275, 300 and 350 m/min (so as to achieve significant wear within a short time), and
- feed-rates: 0.1, 0.2 and 0.3 mm/rev.

6. Experimental procedure

A hand held digital tachometer was used to adjust the cutting speed (V, m/min) on the surface of the workpiece. The required feed-rate (s, mm/rev) was chosen from the lathe pre-set values and the cutting tool wound to the uncut diameter until it just touched the workpiece producing very fine chips at the tool point. This point was taken as the datum from which the desired depth of cut was to be applied. Resetting the charge amplifiers to discard any residual charge, data was then recorded after the tool had been engaged in cutting and sufficient time allowed for a steady state to be attained. Before any experimental data were recorded, the optimum sampling parameters (frequency, number of data samples and the sampling time) were determined. The recorded data consisted of three components of acceleration and cutting forces with sampling performed at a frequency of 30 kHz while recording 4096 data samples per channel.

In this study, mainly interrupted cuts were conducted at fixed cutting conditions with fresh tool inserts until failure or when wear levels had accumulated at which continued cutting risked catastrophic failure (fracture). Due to the rate of tool wear, test cuts generally lasted <10 s at the

beginning of each test run. As the test progressed, the duration of each test was systematically increased to well over 30 s for complete stabilisation of the cutting process to be achieved while at the same time allowing significant tool wear. Each test cut was interrupted after the prescribed time interval to take measurements of flank, nose and notch wear lengths just after the process parameters of interest had been recorded. Tool wear measurements were made using a tool maker's microscope, and the observations supplemented by scanning electron microscope profiling. As well as collecting chip samples, built-up edge and other tool features (chipping or fracture) were noted. The obtained data were analysed in order to investigate the effects wear accumulation had on the sensor signals in terms of their sensitivity and repeatability.

7. Signal analyses

For each test cut performed, a value of static force was calculated from the sampled cutting force, together with an indication of the dynamic force variation. The vibration signals were taken directly as the recorded values of the acceleration signals of the tool holder.

7.1. Static force

The sensor signal processing performed was aimed at extracting features that best described the characteristics of the process conditions. Signals from the metal cutting process generally are non-stationary due to the non-linearity of the cutting process and workpiece non-homogeneity. However, in this part of the study, it was assumed that the cutting static force signal was stationary and independent of time. Therefore, it sufficed to characterise it using power density function, statistical mean (averaging) or time domain indices. The statistical mean of the sampled cutting force was chosen to describe the nature of the static force behaviour since the signal was assumed to be stationary, and its mean therefore remained constant throughout a cutting pass.

For each test cut, the static force component, $\bar{F}$ was calculated as the mean value of the sampled data F_i. The mean value was necessarily taken because the data points continuously varied, thus had no effective value. Therefore, by taking the mean value its statistical variation was inclusive in the ensuing analysis, and was thus justified by the experimentation procedure, i.e.

$$\bar{F}=\frac{1}{N}\sum_{i=1}^{N}F_i(t_i).$$

7.2. Dynamic force and acceleration

With the static force known for each cutting pass, the dynamic or time varying force component for each data point could be determined. If $F_{d(i)}$ represents the dynamic force for the ith data point and the sampled force is F_i, then $F_{d(i)}$ was found as follows:

$$F_{d(i)}=F_i-\bar{F}.$$

Clearly the dynamic force and acceleration signal vary as cutting time progresses, but this was not apparent nor evident on time domain plots as smaller frequency components were masked by bigger ones, but in the frequency domain the whole spectra could be viewed. It was also evident that in the time domain, the signals exhibited dynamic characteristics and behaved in an apparently random manner. The dynamic data (dynamic force and acceleration) were thus transformed from the time to the frequency domain through implementation of an FFT algorithm. The FFT reduced the size of the sampled data and alleviated co-linearity among the dynamic signal components. The processing of the obtained signals in both time and frequency domains was achieved through the versatile Mathwork's Matlab coding programme on a PC. Details of the algorithms and codes appear in the appendices of Dimla [1].

8. Results

Due to limitation of space and the bulky nature of results, only a few plots for experiments conducted with P25 inserts have been presented. Results for P15 were similar to those presented except that the tool life was longer due to its double coating which prolonged tool failure. For comparison and clarity, all the experimental data have been presented in Tables 2 and 3 for P25 ad P15 experiments, respectively. The complete results for both P25 and P15 can be found in Dimla [1].

Inspection of P25 data show that significant changes occurred in the measured parameters as the wear length on the cutting face increased. Increased feed-rate at constant speed decreases tool life by increasing burn-out activity. The same is true for cutting speed changes at constant feed-rate, though more significant in terms of active tool life. DOC was not investigated for reasons outlined earlier.

In total, 7 tests were conducted:

- constant speed (300 m/min) and three feed-rates (0.1, 0.2 and 0.3 mm/rev),
- constant speed (275 m/min) and two feed-rates (0.1 and 0.3 mm/rev),
- constant speed (350 m/min) and two feed-rates (0.1 and 0.3 mm/rev).

Plots of wear (nose, flank and notch) vs. time (Figs. 5–8) were produced together with static force (Figs. 9–11), sum total power (STP) dynamic force (Figs. 12–14), and STP acceleration (Figs. 15–17) relationship with flank wear. Dynamic force and acceleration spectra were produced as well as contour plots (Figs. 18–29).

8.1. Time domain analysis

Wear-time plots mainly highlighted the effective wear rate at the prescribed cutting speed and feed-rate. At low feed-rates, generally the tool wore much gradually than at higher feed-rates. Inspection of these plots showed that it was possible to capture the three phases of tool wear (primary, secondary and tertiary) but only at low feed-rates regardless of cutting speed. In terms of tool life (longevity), the tool lasted longer at low cutting speeds and the wear phases were more visible and pronounced (Fig. 7 cf. Fig. 5, and Fig. 6 cf. Fig. 8). On nearly all the plots, the

Table 2
Experimental results from P25 test cuts

Test No.	Time (s)	Wear (mm)			Static forces (N)			STP dynamic forces(N)			Vibration (g)		
		Notch	Nose	Flank	*x*	*y*	*z*	*x*	*y*	*z*	*x*	*y*	*z*
V=300 and *f*=0.1													
A1	5	0.05	0.01	0.02	301	165	389	87	114	146	79	54	109
A2	12	0.09	0.03	0.05	303	163	384	68	103	129	146	78	99
A3	17	0.11	0.05	0.07	305	167	390	72	96	118	74	53	100
A4	26	0.13	0.06	0.08	306	169	400	75	111	139	75	53	117
A5	34	0.14	0.08	0.1	316	172	433	78	109	136	92	59	113
A6	47	0.15	0.09	0.11	333	180	431	88	128	161	91	66	129
A7	64	0.15	0.1	0.12	332	180	400	82	115	152	74	54	110
A8	82	0.16	0.15	0.13	339	197	385	96	136	174	85	62	122
A9	113	0.16	0.18	0.14	364	208	399	106	125	164	90	65	127
A10	135	0.16	0.2	0.16	374	202	453	111	136	169	90	64	123
A11	155	0.16	0.3	0.21	722	447	520	145	173	245	122	92	205
V=300 and *f*=0.2													
A12	5	0.05	0.02	0.04	343	186	626	147	220	295	127	97	226
A13	12	0.07	0.05	0.06	346	187	636	148	250	311	130	98	229
A14	22	0.09	0.07	0.07	349	183	617	128	218	273	118	92	216
A15	34	0.11	0.08	0.1	356	190	624	126	221	252	138	99	239
A16	47	0.14	0.11	0.13	384	199	684	137	236	284	153	108	254
A17	66	0.16	0.13	0.15	428	223	668	153	249	310	154	115	267
A18	79	0.17	0.16	0.17	449	248	680	170	263	333	159	108	272
A19	95	0.17	0.18	0.19	501	286	675	173	281	357	144	105	260
A20	103	0.17	0.21	0.2	550	318	657	168	270	339	146	100	245
A21	115	0.17	0.35	0.22	771	536	727	181	277	333	167	108	276

(continued on next page)

most noticeable indicator of imminent tool failure was the sudden escalation of nose wear to failure. Typically, when the nose wear was higher than 0.2 mm, one ran the risk of catastrophic failure. This level of wear was also found to be an applicable safety threshold for the flank wear length. Notch wear on the other hand increased steadily in the early part of the tests, then remained practically the same for the remainder of tool life.

8.1.1. Static force

The table of results show that the static force generally increased, albeit slightly, as the wear on the cutting tool face increased, for both increases in feed-rate and cutting speed. A closer inspection of the obtained figures for the static force-flank wear relationship reveals a variable but increasing trend in all three axes (Figs. 9–11). Fig. 9 shows that beyond a flank wear length of 0.15 mm, the cutting forces increased by nearly 200%.

8.1.2. StP dynamic signals

- Dynamic force: Generally, at low feed-rates, the initial trend was upward (Fig. 12) and then fell when a flank wear length of 0.2 mm was exceeded. The other figures tended to depict a

Table 2 (*continued*)

Test No.	Time (s)	Wear (mm)			Static forces (N)			STP dynamic forces(N)			Vibration (g)		
		Notch	Nose	Flank	*x*	*y*	*z*	*x*	*y*	*z*	*x*	*y*	*z*
V=300 and *f*=0.3													
A22	8	0.04	0.02	0.03	435	238	988	378	606	784	344	228	642
A23	21	0.1	0.08	0.12	468	259	999	316	637	749	293	212	571
A24	32	0.11	0.14	0.15	538	304	1038	333	667	790	325	218	597
A25	50	0.15	0.15	0.16	602	370	1096	359	738	831	352	238	651
A26	62	0.17	0.22	0.18	608	431	1037	333	600	733	367	230	640
A27	73	0.17	0.24	0.19	649	530	1073	352	623	757	368	244	667
A28	83	0.17	0.4	0.2	790	1211	1172	364	633	833	408	278	748
V=275 and *f*=0.1													
A29	9	0.03	0.01	0.02	295	169	435	90	138	162	102	59	126
A30	17	0.06	0.03	0.05	296	169	443	89	135	160	100	64	126
A31	29	0.09	0.07	0.08	297	166	446	82	128	150	97	60	126
A32	42	0.1	0.09	0.09	291	171	435	90	134	165	104	71	141
A33	56	0.11	0.1	0.1	301	176	430	101	141	183	107	68	138
A34	75	0.12	0.11	0.11	302	172	439	98	141	170	114	69	143
A35	100	0.13	0.13	0.12	297	175	441	108	145	170	91	64	136
A36	123	0.14	0.13	0.13	297	169	442	114	160	210	93	69	141
A37	159	0.15	0.14	0.14	301	176	439	120	175	214	100	70	146
A38	181	0.16	0.16	0.15	300	172	423	115	149	198	110	66	132
A39	220	0.17	0.17	0.16	307	175	446	119	152	204	117	71	143
A40	253	0.18	0.18	0.17	306	178	460	112	164	211	102	75	158
A41	313	0.2	0.19	0.18	299	170	436	120	163	207	108	77	158
A42	403	0.21	0.2	0.19	298	168	473	126	176	226	117	90	189
A43	479	0.21	0.22	0.21	291	176	452	111	164	215	98	80	173
A44	569	0.21	0.27	0.24	303	169	464	100	167	187	106	79	165
V=275 and *f*=0.3													
A45	3	0.01	0.04	0.02	439	235	1081	378	595	769	459	259	653
A46	13	0.07	0.06	0.07	461	240	1102	333	605	739	379	240	610
A47	24	0.08	0.1	0.1	493	255	1028	360	679	863	394	260	655
A48	35	0.12	0.12	0.12	504	265	1010	340	632	812	392	254	687
A49	45	0.13	0.13	0.14	538	281	1045	348	632	784	377	260	660
A50	53	0.15	0.14	0.15	551	297	1029	355	631	747	386	263	681
A51	64	0.15	0.15	0.16	576	310	1062	361	670	821	429	283	750
A52	76	0.15	0.16	0.17	613	347	1051	378	704	894	414	274	746
A53	98	0.15	0.17	0.18	643	385	1078	358	676	838	433	275	737
A54	119	0.15	0.18	0.19	670	422	1067	346	669	835	403	257	677
A55	139	0.15	0.2	0.2	662	428	1060	342	653	810	407	262	681
A56	157	0.15	0.23	0.22	683	465	1095	377	728	892	444	267	746
A57	192	0.15	0.37	0.3	832	823	1179	392	689	907	506	278	776

Table 3
Experimental results from P15 test cuts

Test No.	Time (s)	Wear form (mm)			Static force (N)			STP dynamic force (N)			STP acceleration (g)		
		Notch	Nose	Flank	*X*	*Y*	*Z*	*X*	*Y*	*Z*	*X*	*Y*	*Z*
V=300 and *f*=0.1													
B1	13	0.04	0.03	0.05	352	188	423	105	143	160	94	64	126
B2	28	0.06	0.06	0.07	348	182	436	83	121	139	73	56	121
B3	46	0.07	0.07	0.09	362	197	453	117	162	186	90	64	149
B4	64	0.08	0.09	0.1	362	201	448	108	152	184	96	66	137
B5	101	0.09	0.1	0.11	370	210	458	103	143	171	108	65	133
B6	134	0.1	0.1	0.12	383	208	446	114	156	182	105	73	144
B7	167	0.11	0.1	0.13	375	209	471	114	154	179	104	67	125
B8	212	0.12	0.1	0.14	401	232	498	106	161	178	92	69	136
B9	274	0.12	0.1	0.15	407	220	464	119	157	179	63	69	146
B10	319	0.12	0.1	0.16	394	207	484	109	142	173	111	68	136
B11	376	0.12	0.1	0.17	392	223	472	106	156	175	91	66	133
B12	425	0.12	0.1	0.18	395	214	504	114	162	176	65	74	164
B13	528	0.12	0.12	0.19	368	195	484	107	165	187	50	75	183
B14	654	0.12	0.13	0.2	354	187	478	110	166	197	99	78	189
B15	775	0.12	0.14	0.21	331	175	459	108	152	186	82	71	179
B16	1006	0.12	0.15	0.22	317	167	432	100	169	196	82	79	171
B17	1113	0.12	0.17	0.24	309	169	428	110	174	200	75	76	175
B17R	1185	0.12	0.18	0.26	319	155	479	119	184	219	87	86	175
V=300 and *f*=0.3													
B18	9	0.03	0.04	0.06	533	299	1011	451	769	1006	300	319	860
B19	20	0.05	0.08	0.1	557	299	1033	366	635	851	309	364	737
B20	35	0.07	0.11	0.13	591	330	1064	381	716	911	272	267	780
B21	74	0.12	0.16	0.19	723	441	1098	397	729	914	289	293	820
B22	123	0.15	0.17	0.28	951	659	1134	402	709	940	310	289	808
B23	150	0.15	0.25	0.35	1185	953	1240	394	667	865	358	378	735
V=275 and *f*=0.3													
B24	8	0.04	0.02	0.05	462	249	947	511	698	1058	308	461	838
B25	33	0.06	0.08	0.09	586	283	1111	383	656	863	312	410	760
B26	84	0.08	0.11	0.1	588	310	1013	360	673	814	308	352	666
B27	134	0.12	0.13	0.11	660	350	1078	365	618	753	370	327	608
B28	180	0.13	0.14	0.18	727	401	1024	365	620	783	344	333	653
B29	224	0.15	0.17	0.25	798	450	1058	386	664	802	317	342	685
B30	268	0.15	0.19	0.27	865	493	1124	395	667	805	123	353	673

rather undulating behaviour, for which interpretation was difficult and frequency analysis required.

- Acceleration (vibration signature): Increases in flank wear lead to proportional increments in the STP acceleration signals, peaking at a flank wear length of 0.2 mm before gradually falling. This trend was most noticeable when cutting at high speed and feed-rates (Figs. 15–17). Again, examining the time domain plots could not make clear and meaningful observation.

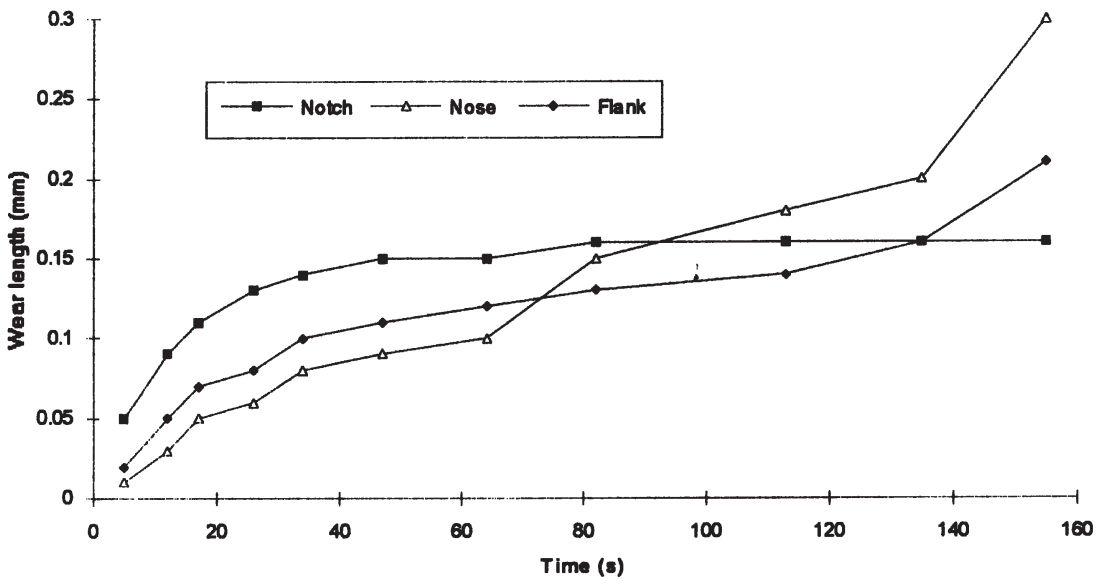

Fig. 5. Wear–time plot (V=300 m/min and f=0.1 mm/rev).

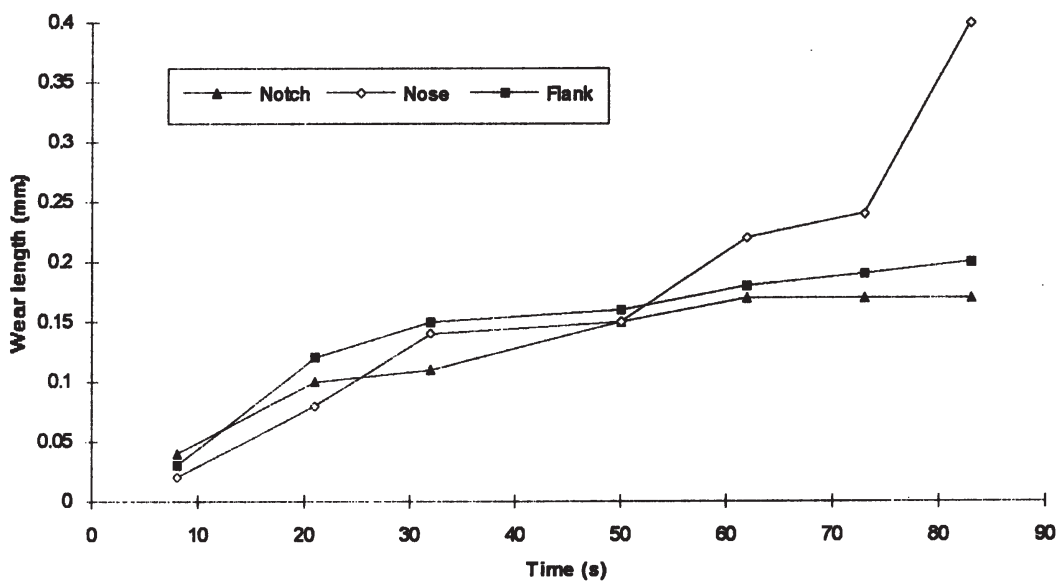

Fig. 6. Wear–time plot (V=300 m/min and f=0.3 mm/rev).

8.2. Frequency analysis

Frequency analysis involved performing a forward FFT on the data, and the results interpreted through two media: spectra and contour plots. With spectra plots it was possible to visualise

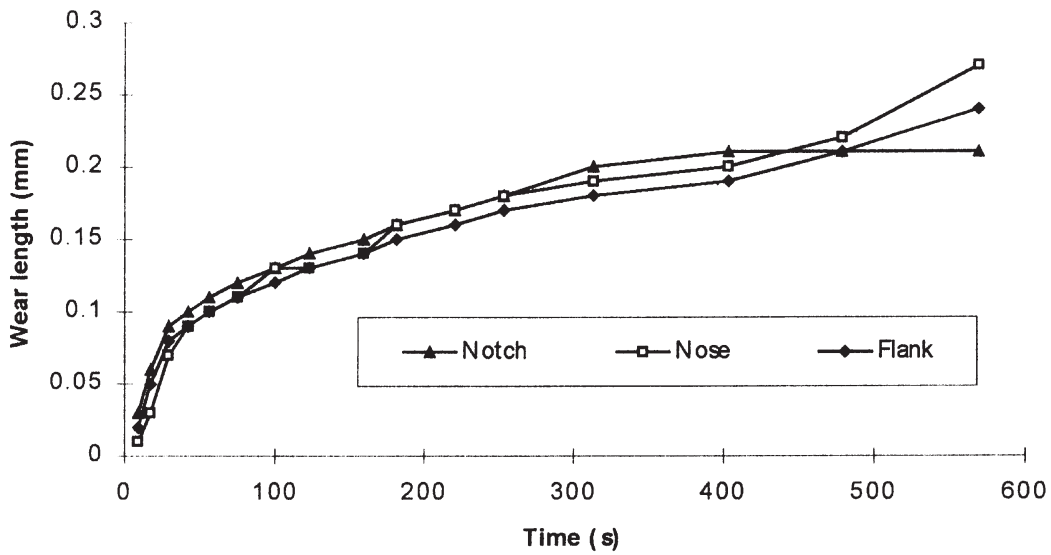

Fig. 7. Wear–time plot (V=275 m/min and f=0.1 mm/rev).

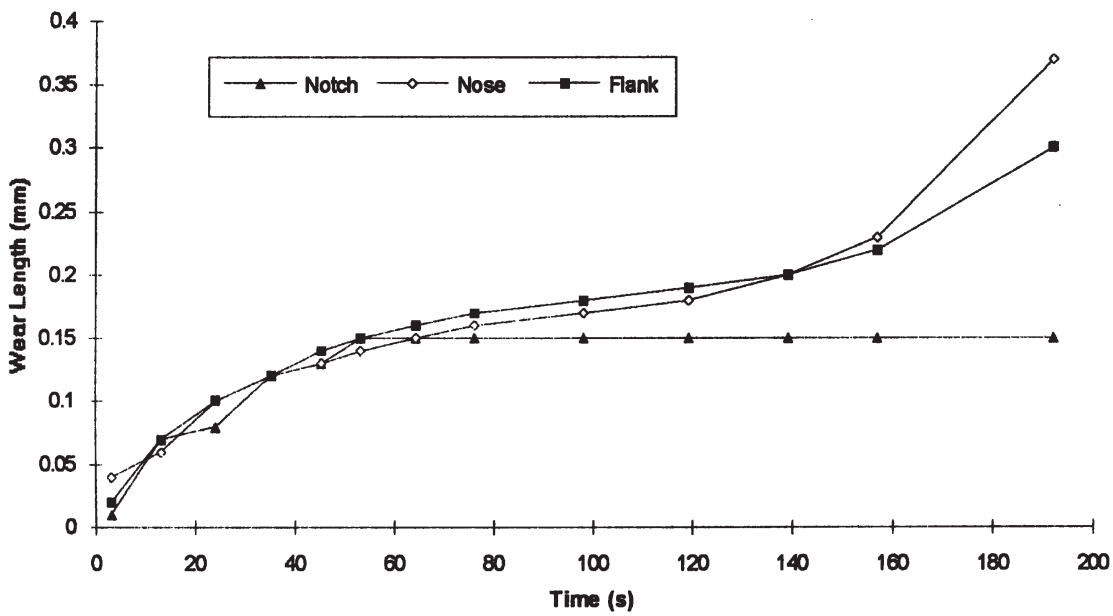

Fig. 8. Wear–time plot (V=275 m/min f=0.3 mm/rev).

significant amplitude variations and their corresponding frequencies, whereas the overall frequency bands were better viewed on a contour plot.

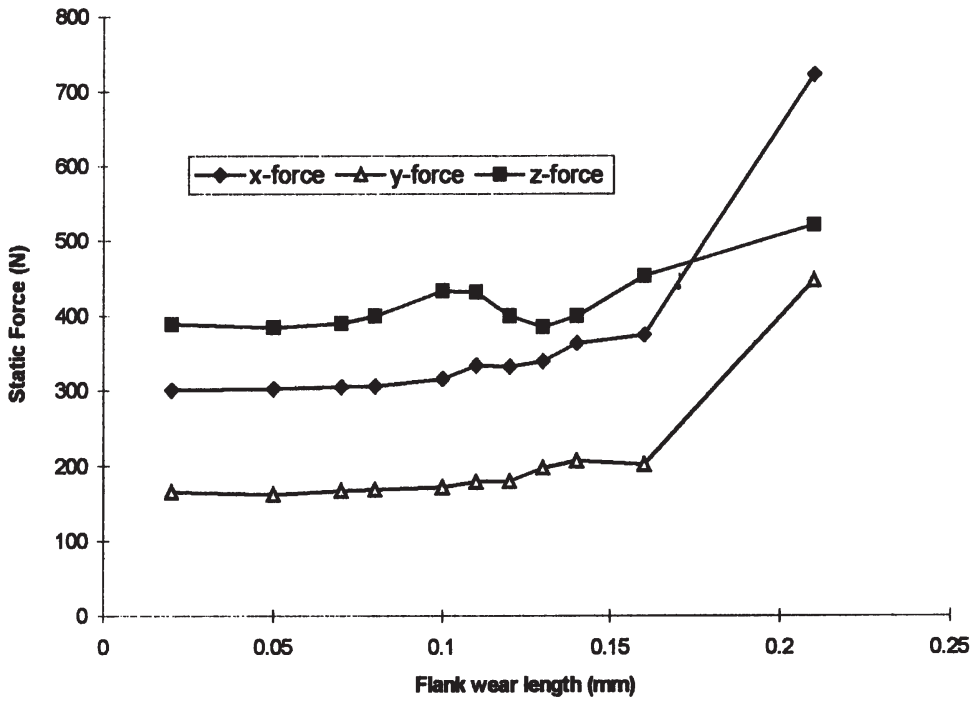

Fig. 9. Static force–flank wear (V=300 m/min and f=0.1 mm/rev).

8.2.1. Dynamic force

8.2.1.1. Spectra plots The spectra plots (Figs. 18–20) generally showed three principal frequency bands that could be associated with wear accumulation. However, inspection of the x-axis spectra showed peaks at 500 Hz, 1500 Hz, 3–4 kHz and 10 kHz. The 3–4 kHz frequency peak was the most sensitive to wear levels which coincided with the dynamometer resonant frequency. This main peak remained constant for the first three wear values (primary wear) showing minor signs of oscillation with rapid increase in flank and nose wear. Once the wear values reached 0.1 mm, the wear increment was rather gradual with the contact area staying relatively the same. The increase in peak value beyond the 4th test run could be attributed to an increase in flank wear. The increase in peak height was not proportional to either the flank or nose wear value. Thus, the sensitive peak initially rose with wear accruement, then fell as the tertiary wear phase was reached with the peaks falling as damping occurred.

These observations were more pronounced on the low feed-rate plots (0.1 mm/rev) and less at high feeds (0.3 mm/rev). The dramatic rise in the 10 kHz peak towards tool failure reflected the rapid increase in the nose and flank wear values, which in most instances coincided with tool chipping.

8.2.1.2. Contour plots Inspection of the plots (Figs. 25–27) showed three main dominant peak frequencies. At low feed, the x-axis plot had peaks at 500 Hz, 1.5–2 kHz and 3.5–4 kHz frequency bands. On the y- and z-plots, the main energy concentrated in the 2–3 kHz frequency band with

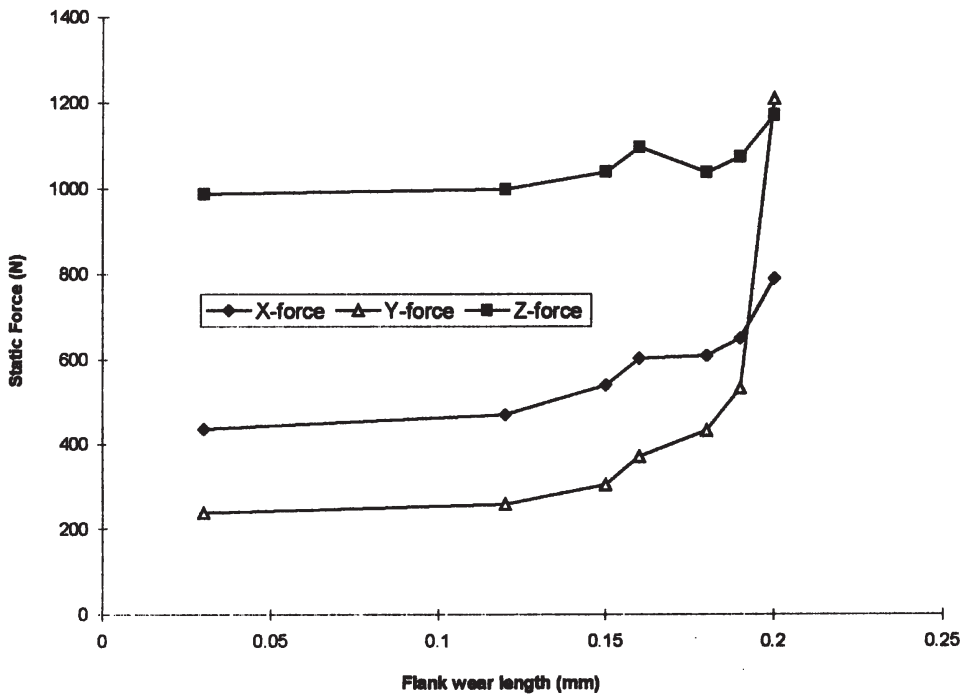

Fig. 10. Static force–flank wear (V=300 m/min and f=0.3 mm/rev).

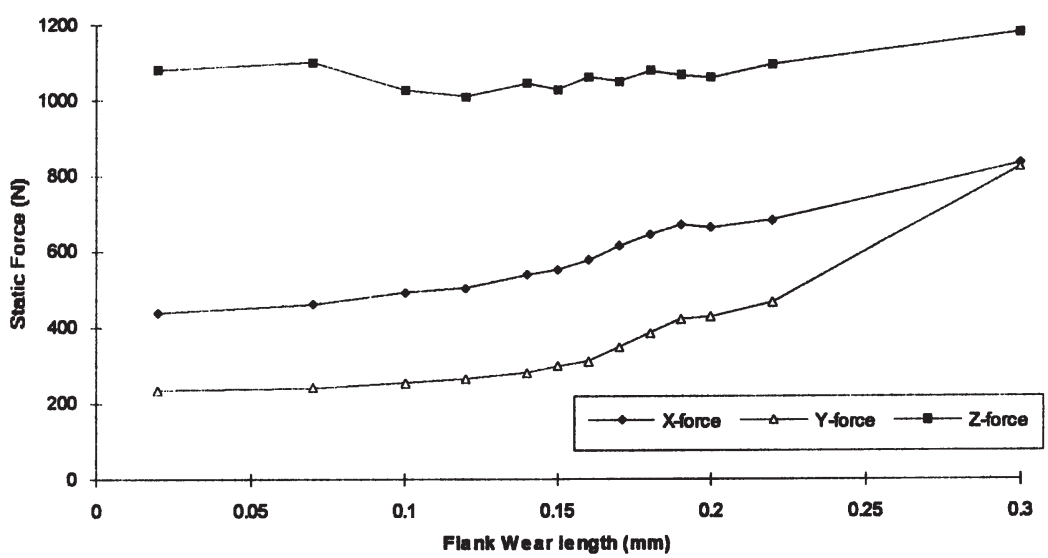

Fig. 11. Static force–flank wear (V=275 m/min and f=0.3 mm/rev).

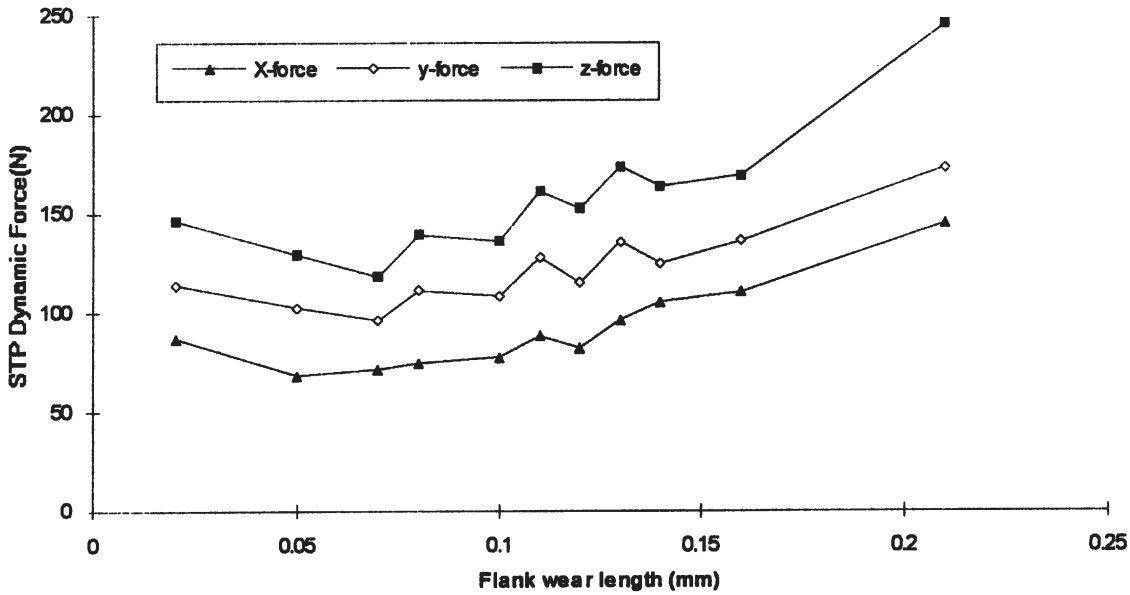

Fig. 12. STP dynamic force spectra–flank wear (V=300 m/min and f=0.1 mm/rev).

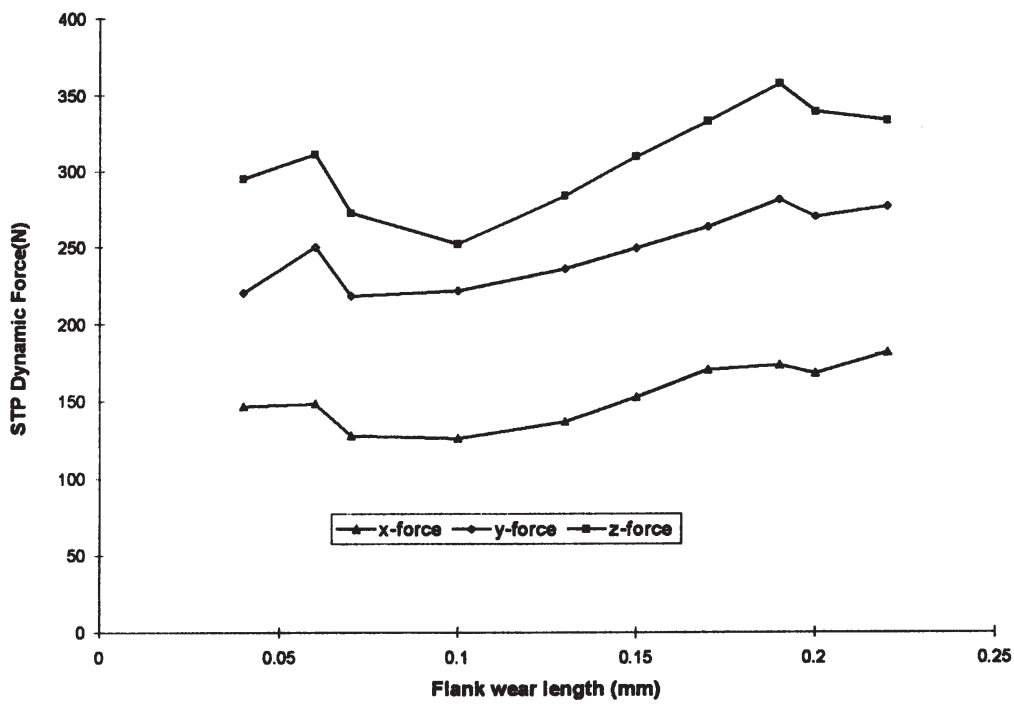

Fig. 13. STP dynamic force spectra–flank wear (V=300 m/min and f=0.2mm/rev).

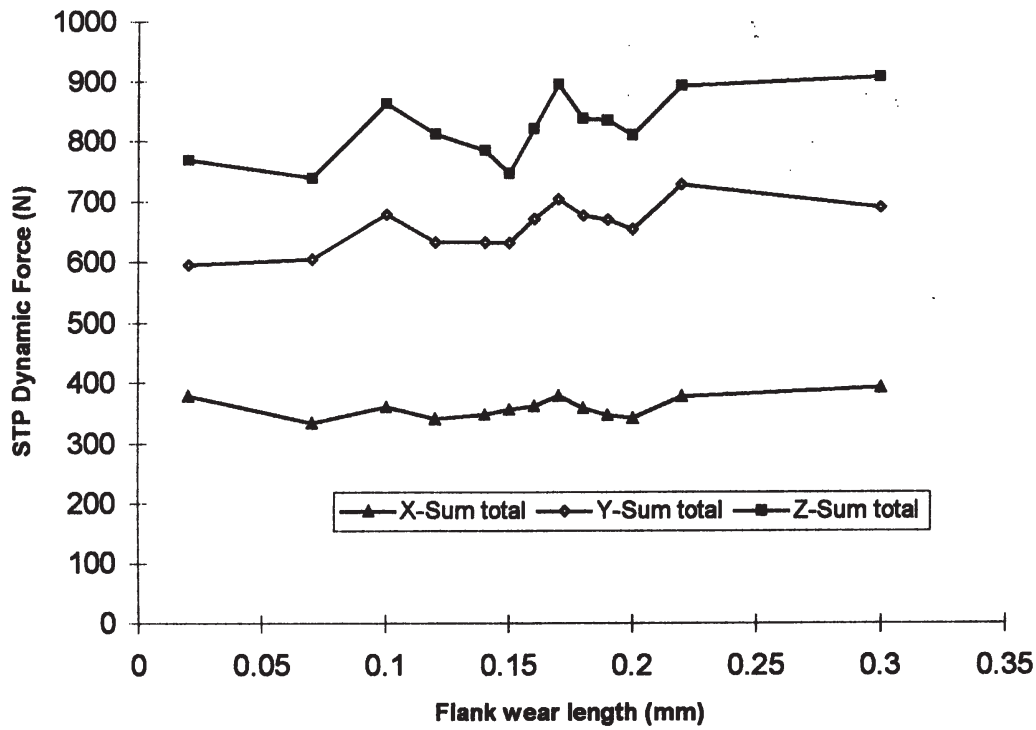

Fig. 14. STP dynamic force spectra–flank wear (V=275 m/min and f=0.3 mm/rev).

a slight energy concentration appearing at ≈11 kHz. Increases in the feed-rate caused the spectra to become dispersed with the low frequency band disappearing.

8.2.2. Vibration signal

8.2.2.1. Spectra plots Unlike the dynamic force spectra, the vibration spectra (Figs. 21–24) had two main peak frequency bands: a 2–4 kHz (the fundamental resonant frequency of the tool holder) and a 9–11 kHz band (chip lamination frequency). Inspection of the plots revealed the z-axis plots to be the most sensitive to wear increment. The 2–4 kHz band increased steadily peaking before falling to reach tool failure. Meanwhile, the 9–11 kHz peak increased as wear increased with the last spectrum showing the largest increase. Increases in the feed-rate led to a proportional increase in the magnitude of both peaks, indicating the same trend as with low feeds. However, at high feed-rates, the spectra were noisier and had a wider frequency band. Comparison of spectra depicting cutting at different cutting speed showed that increasing the cutting speed actually decreased the amplitudes of the resonant peak.

8.2.2.2. Contour plots These plots (Figs. 28 and 29) clarified observations made from the spectra plots, i.e. that there existed two principal frequency peaks; a low band ≈3 kHz and a higher and larger energy concentration band at 10–12 kHz. No effects of tool wear were visible, but feed-rate and cutting speed increases tended to generally increase the energy and noisy nature of

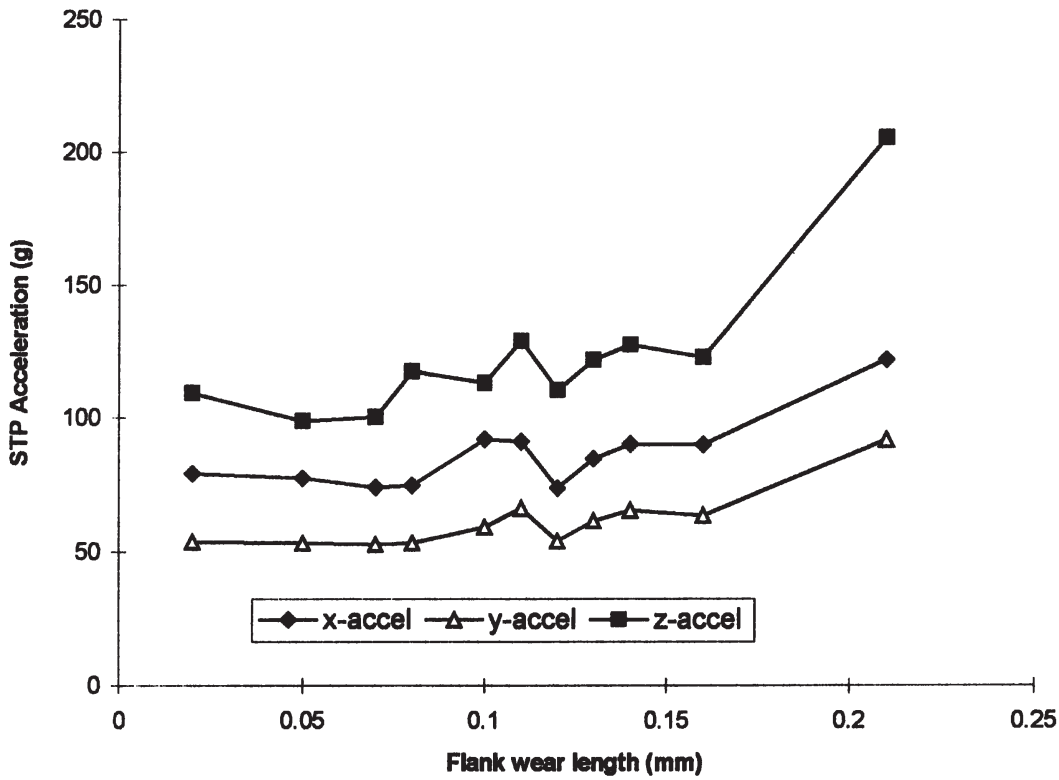

Fig. 15. STP acceleration spectra–flank wear (V=300 m/min and f=0.1 mm/rev).

the contour. For example, increasing the cutting speed from 275 to 300 m/min. introduced a low band spectrum at 2.5–3 kHz on the z-vibration at 0.1 mm/rev feed-rate. At high feed-rates, these merely became sharp with smaller bandwidths corresponding to higher cutting speeds.

9. Discussion and comparison of P15 and P25 results

Due to the complex and stochastic nature of the cutting process, identification of the exact or actual tool condition was difficult. During the experimental stages of the wear progression studies, it was noted that some tool inserts failed at considerably small flank wear lengths. The most likely explanation to account for these failures were partly attributed to what might be called "thermally induced premature failure mechanism" [21]. A common characteristic to these occurrences was that a majority of the failures tended to occur at high cutting speeds (i.e. 350 m/min). A possible shortcoming in these investigations was the relative difficulty to accurately measure the flank, nose and notch wear lengths especially when they were irregular. The reported wear values were therefore prone to error. It should be remembered that quoted wear values would be expected to deviate from the true or ideal values due to the element of subjectivity. Owing to the irregularity of the major flank wear region, the maximum flank wear length (V_{BMax}) was used as the standard measure of flank wear length. This was because at certain levels of wear, the previously uniform

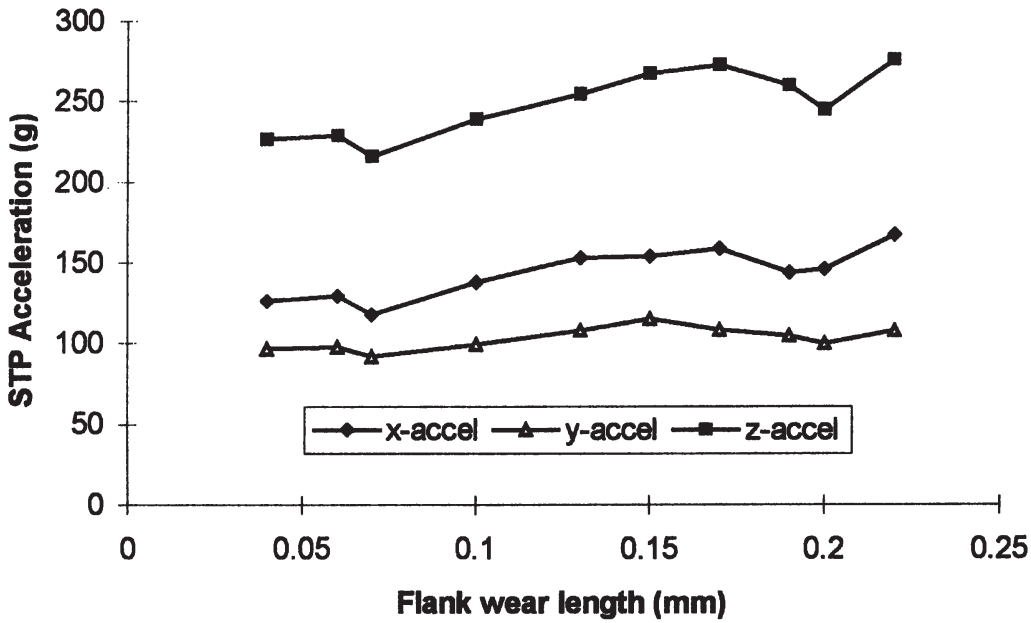

Fig. 16. STP acceleration spectra–flank wear (V=300 m/min and f=0.2mm/rev).

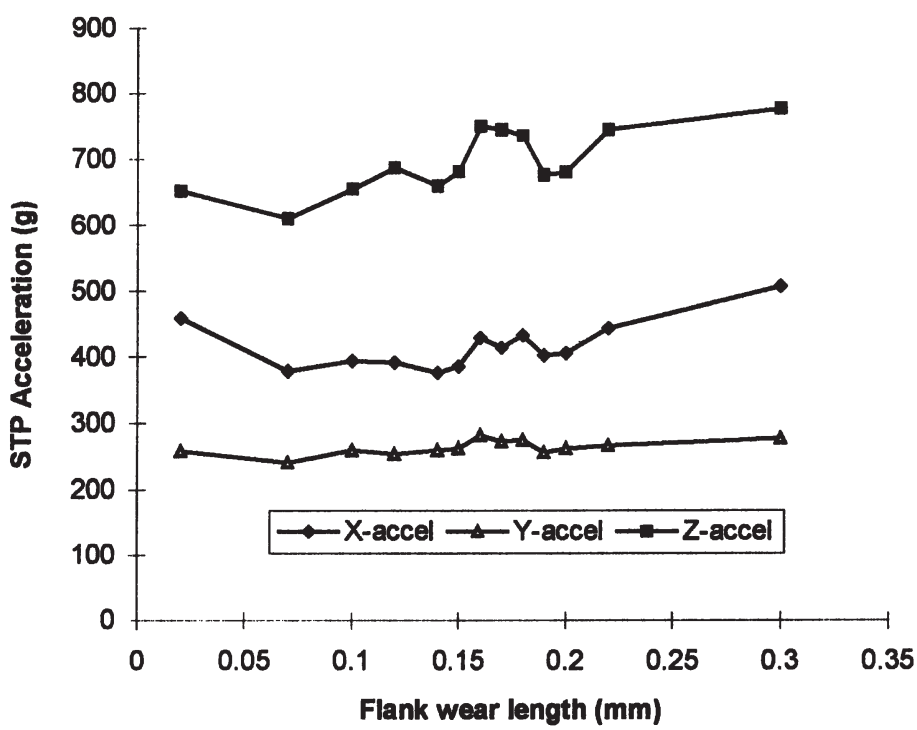

Fig. 17. STP acceleration spectra–flank wear (V=275 m/min and f=0.3 mm/rev).

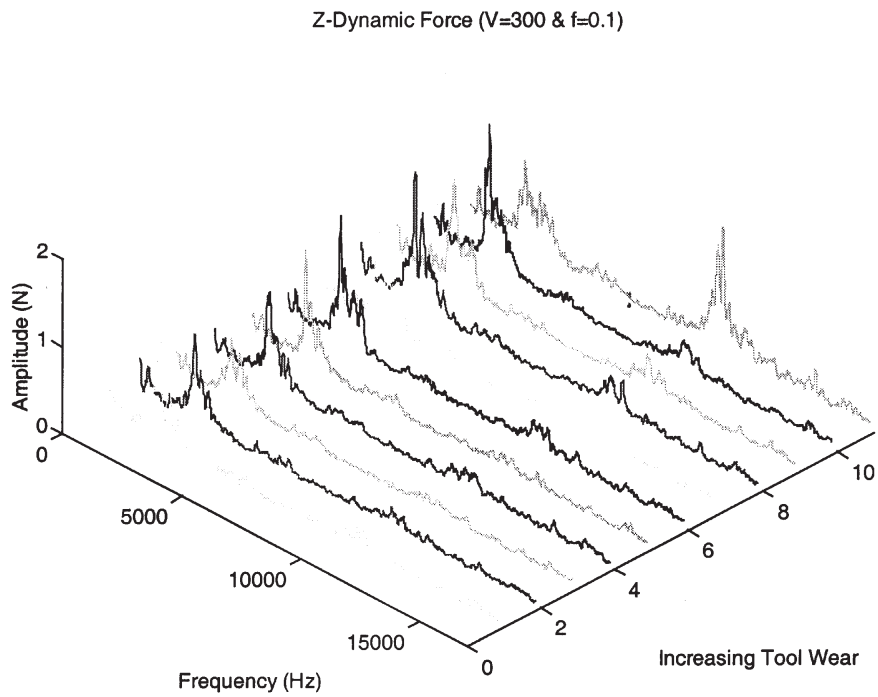

Fig. 18. Z-dynamic force spectra–flank wear (V=300 m/min and f=0.1 mm/rev).

wear cross-section region (at low flank land length) suddenly became non-uniform and accurate measurements were impossible. In almost all the tests conducted, it was found that, the end of tool life was indicated by the sudden escalation of both the flank and nose wear land lengths. These usually were accompanied by large scale increases and fluctuations in the magnitude of the static cutting forces that was attributed to bulk deformation brought about by mechanical and thermal effects [3].

Generally, when cutting took place at low feed-rates, the static cutting forces decreased very slightly as cutting time progressed due to increased wear levels. The decreasing static cutting forces approached a stationary value which was found to be dependent upon the amount of flank and nose wear present, and also on the nature of the tooling material. This behaviour was rather more difficult to ascertain with the P15 insert than with the P25. Principally, a noticeable difference in the two insert types was the occurrence of the so-called built-up edge (BUE) effect. While considerable BUE occurred in the P25, little or no BUE occurred when machining with the P15 insert regardless of cutting speed, feed-rate or wear levels. A common occurrence to both insert types was the fact that beyond the stationary wear value, nose wear was found to rise at a faster rate than flank wear land length. This seemed to suggest that catastrophic tool failure occurred largely at the tool nose, and nose wear perhaps was a better indicator of end of tool life. Chipping of the cutting edge often accompanied such dramatic rise in nose wear length. Oraby and Hayhurst [17] attributed tool failure as actually originating at the nose then triggering failure from either the flank or notch areas. Observations from these experiments seem to concur with that view, but only in so far as nose and flank wear were concerned. No evidence was found to suggest that

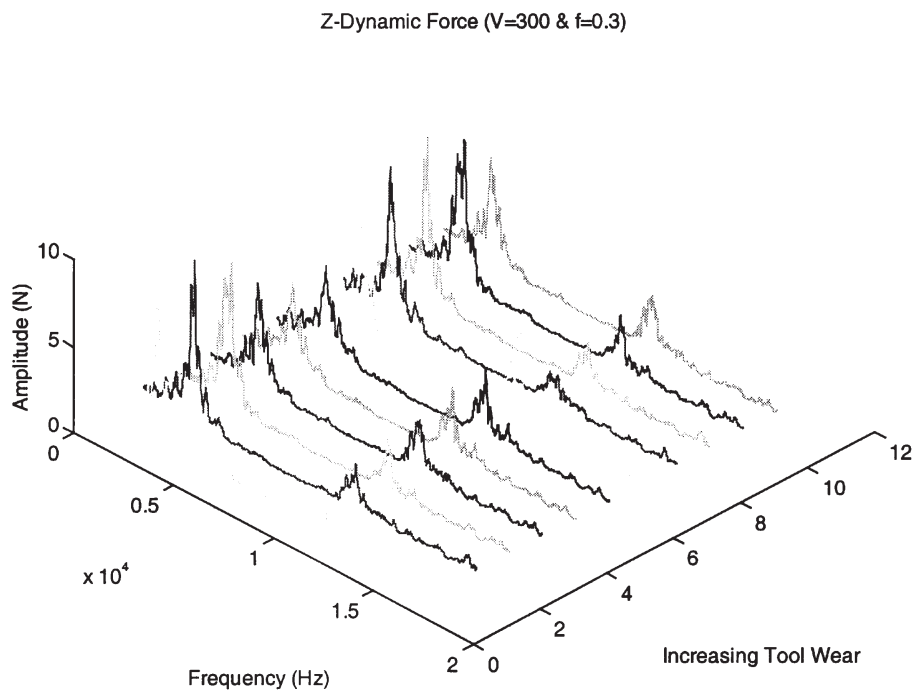

Fig. 19. Z-dynamic force spectra–flank wear (V=300 m/min and f=0.3 mm/rev).

tool failure might have been triggered by flank face notch wear. Under such circumstances, it would be possible to use nose wear to signal the end of tool life and its imminent replacement. A practical approach would be to track both flank and nose wear levels and know exactly which wear regime the tool was in (i.e. its wear phase). Then the rise in nose wear would signal the approach of the catastrophic failure region and therefore, an ideal time to replace the tool insert. The limitations of using static forces alone include disturbances on their magnitude arising from variations in the workpiece material, DOC, feed-rate and possibly tool edge geometry. In practical applications such as a TCMS, it is prudent to supplement tool wear information by using signals from other sources particularly those that indicate the dynamic characteristics of the cutting process. The primary motive for this suggestion hinges on the fact that the aforementioned variations can result in the static forces magnitudes changing in the same order as those due to tool wear effects. It was therefore thought necessary to examine the nature of both kinematics describing quantities viz.: the dynamic cutting force spectra and the vibration signature spectra and their correlation to wear levels assessed.

The method used for evaluating the vibration signatures and the dynamic cutting force signals involved the transformation of the measured signals from time to frequency domain by FFT. Through this method, it was possible to view properties or characteristic information of the cutting process hidden in the time domain. Since tool wear features on the signals were of prime importance, the analysed and presented spectra began with those describing the tool characteristics at first contact (i.e. when tool was new and therefore sharp). This then ended with those spectra describing the severely worn tool characteristics (or the occasional chipping/failure modes). From

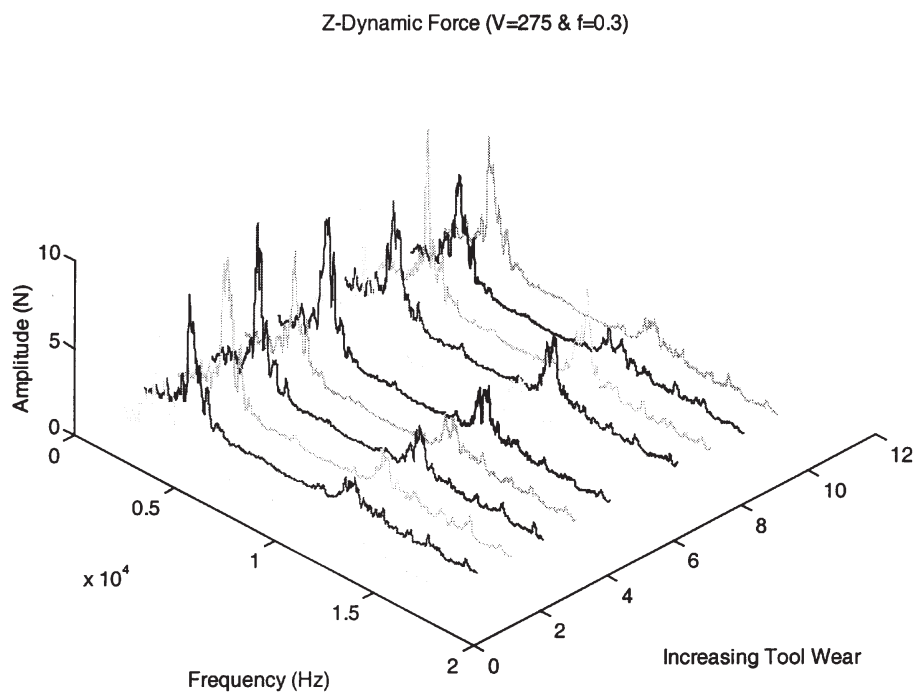

Fig. 20. Z-dynamic force spectra–flank wear (V=275 m/min and f=0.3 mm/rev).

the spectra obtained, it was possible to establish a distinct difference in signal characteristics when cutting was performed with a new insert compared to that which had accrued a detrimental level of wear. The characteristic rise in amplitude of the fundamental resonance frequency peak of the dynamic force signal was attributed to the cyclical stick-slip effect in the contact area. The physics of this effect is due mainly to the fact that when the tool is sharp (i.e. new), the sharp edges minimise contact between the tool and workpiece. This results in small movements, hence small dynamic forces indicated on the spectra by peak magnitudes at the resonant frequency on the spectra. Increasing wear levels led to an increase in the contact area due to crumbled cutting edges. The transition of friction from static to sliding generates high signal pulses that contribute to increasing the magnitude of the fundamental resonant peak as well as appearing as secondary peaks around the 10 kHz band region. Beyond a certain flank wear value, the fundamental frequency peak begins to dampen as the contact area increases monotonically, partly due to increased contact friction and thereof plastic deformation and the development of accelerated nose wear. It could therefore be argued that the occurrence of monotonic nose wear causes the resonant peak magnitude to decrease. Inspection of the chips formed indicated that the high burst was due to increases in the lamination frequency (from $>$1 kHz to around 10 kHz). Increases in the lamination frequency arose from the change in deformation behaviour of the material in the shear zone. A theoretical base for the decline in resonant frequency peak amplitude when the tool was severely worn could be due to an increase in the rake angle from the rubbing effect of the deformed chip [22,23].

Since the dynamic force and vibration signature consist mainly of a combination of stochastic,

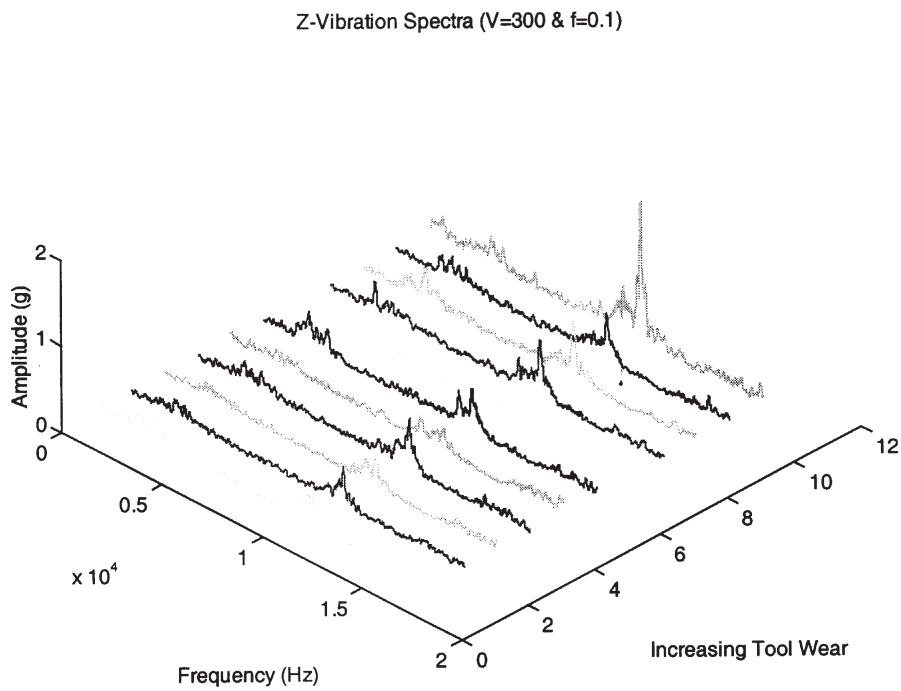

Fig. 21. Z-acceleration spectra–flank wear (V=300 m/min and f=0.1 mm/rev).

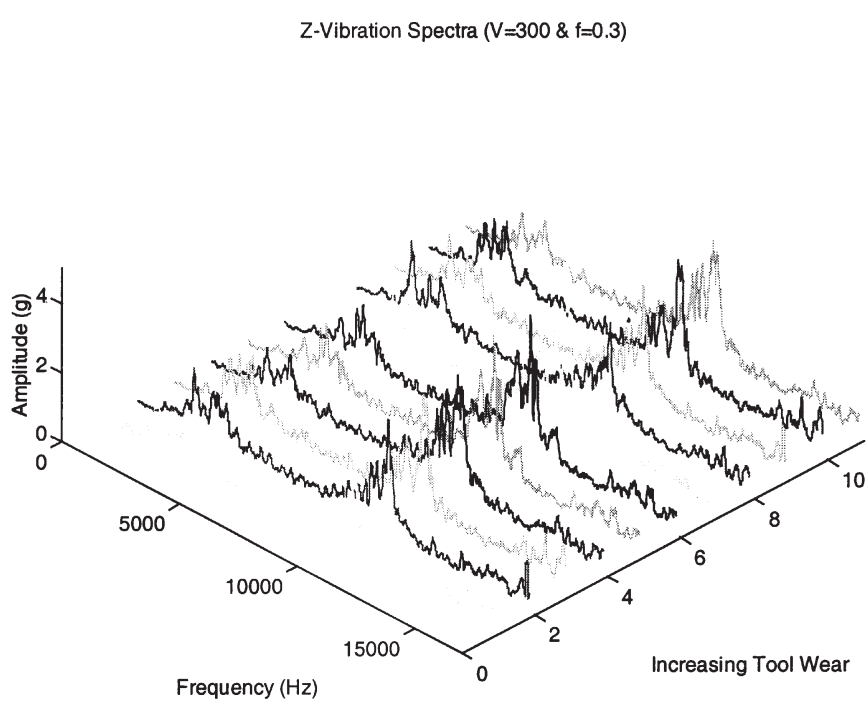

Fig. 22. Z-acceleration spectra–flank wear (V=300 m/min and f=0.3 mm/rev).

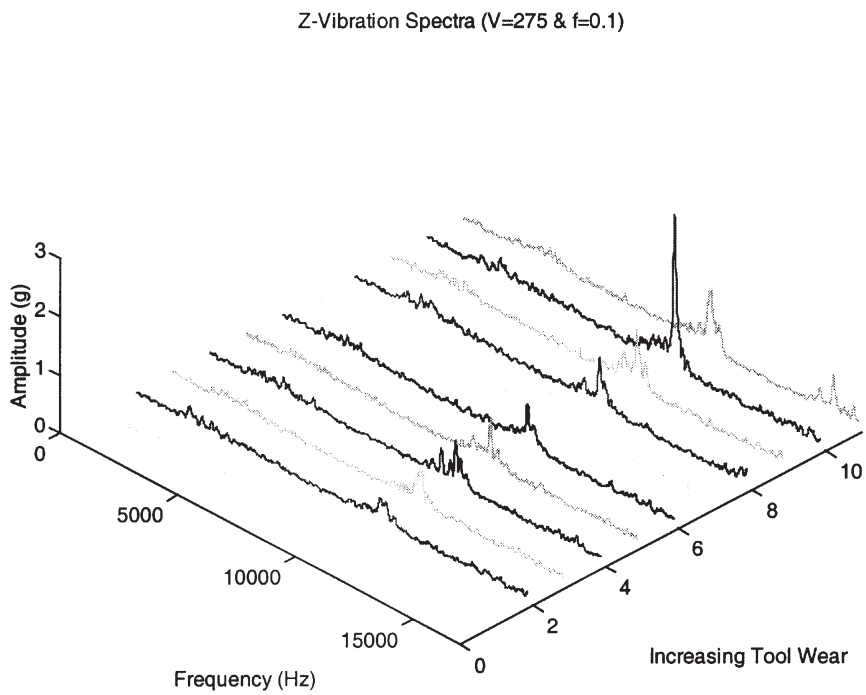

Fig. 23. Z-acceleration spectra–flank wear (V=275 m/min and f=0.1 mm/rev).

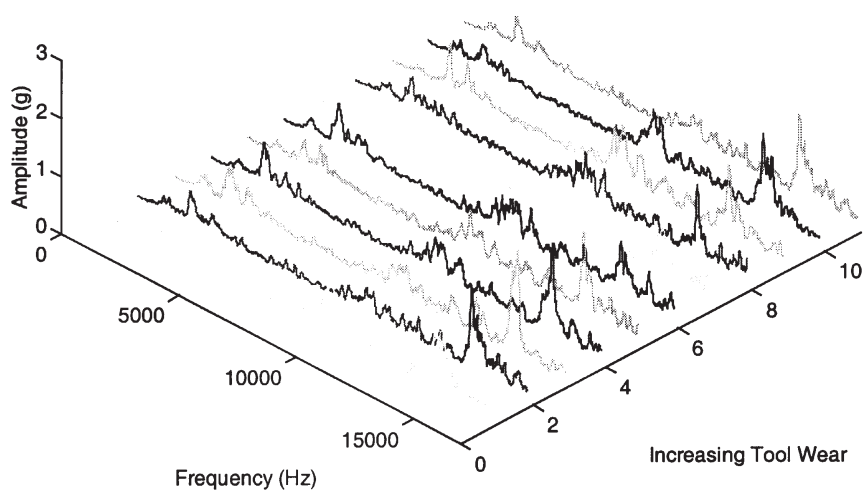

Fig. 24. Y-acceleration spectra–flank wear (V=275 m/min and f=0.3 mm/rev).

periodic and superposed harmonic signals [24], a method of observation that combines both aspects of signal and process behaviour was desired. The computation of the sum total power contained in each sampled signal by adding up all the FFT points seemed the best, logical, and most appropriate approach. This approach delivered the probability that the most significant properties affected by increased wear on the tool surface was inclusive in the analysed signal.

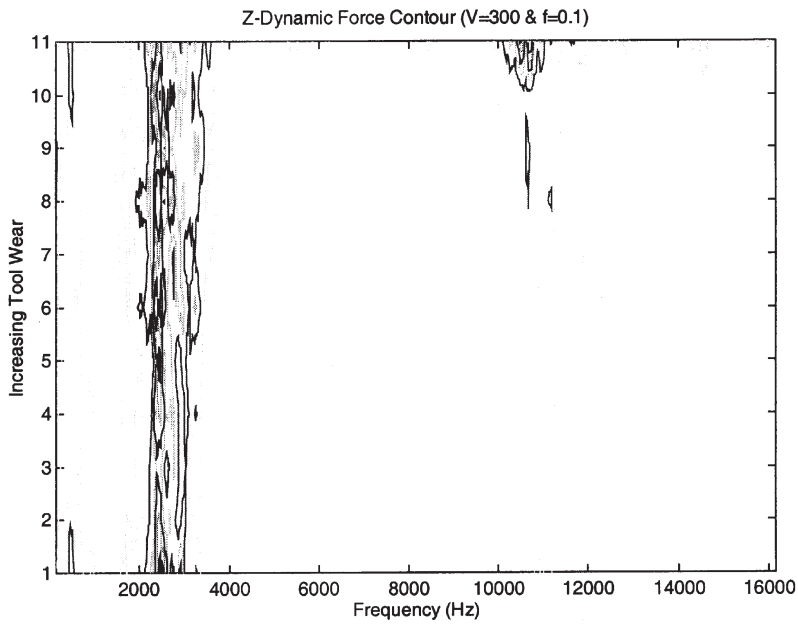

Fig. 25. Z-dynamic force contour (V=300 m/min and f=0.1 mm/rev).

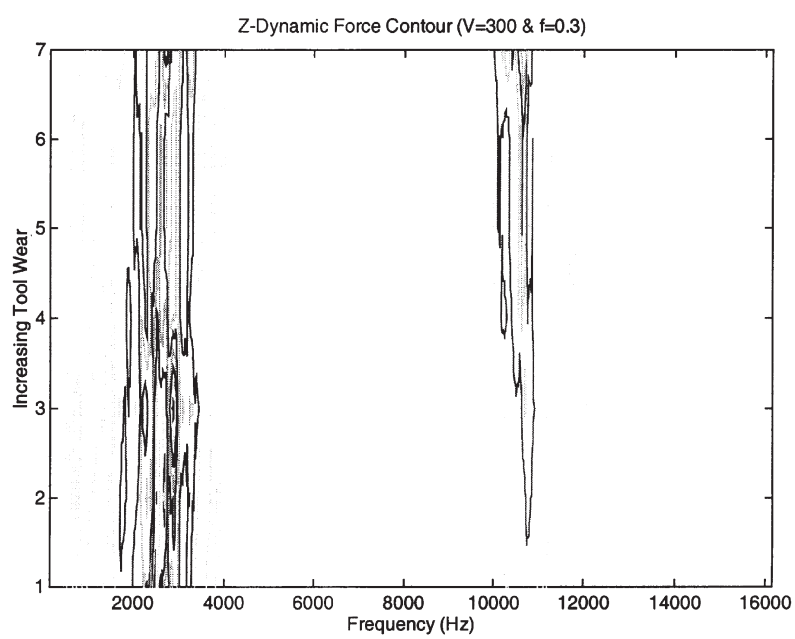

Fig. 26. Z-dynamic force contour (V=300 m/min and f=0.3 mm/rev).

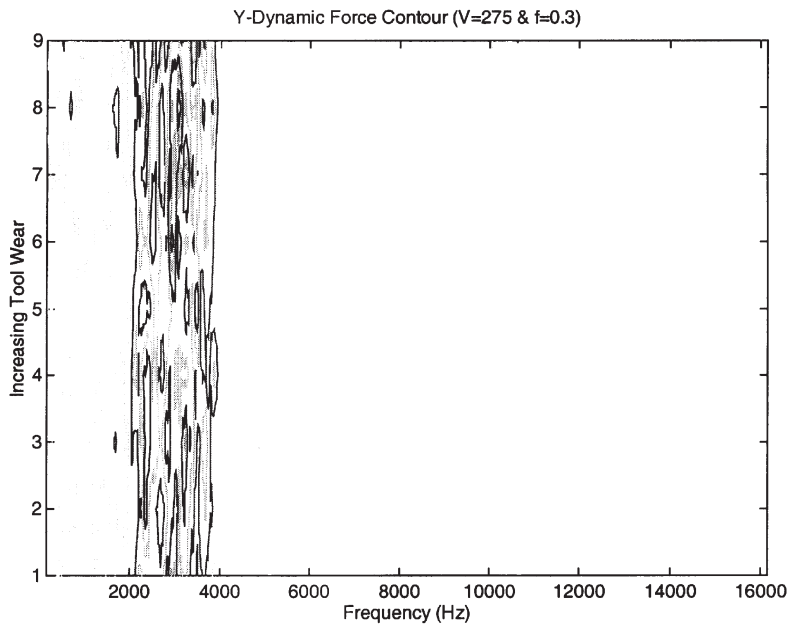

Fig. 27. Y-dynamic force contour (V=275 m/min and f=0.3 mm/rev).

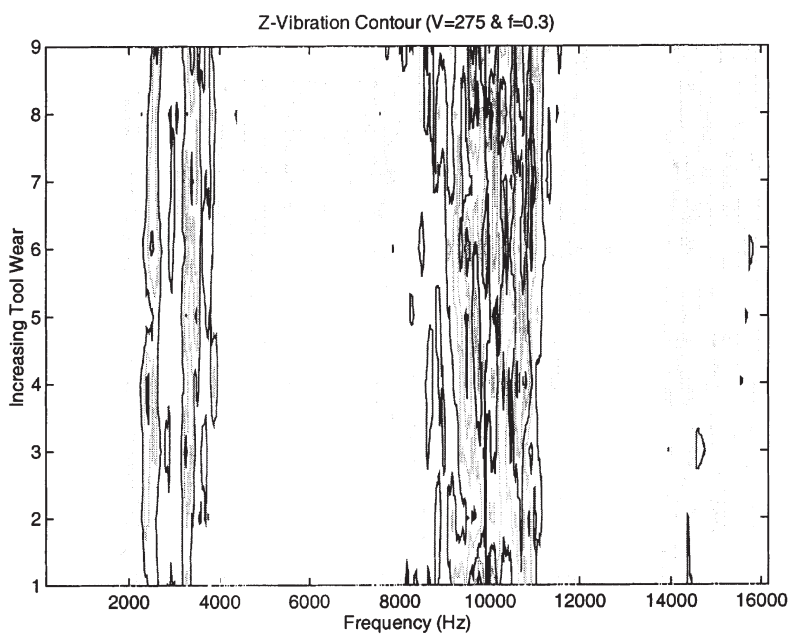

Fig. 28. X-acceleration contour (V=300 m/min and f=0.3 mm/rev).

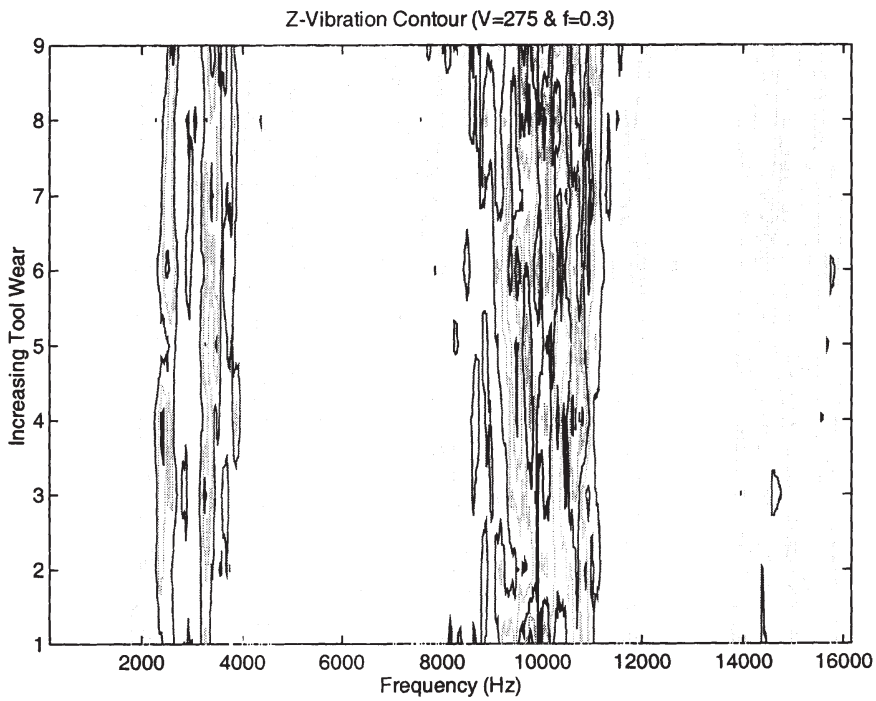

Fig. 29. Z-acceleration contour (V=275 m/min and f=0.3 mm/rev).

10. Conclusions

An experimental tool wear monitoring method based on multivariate analysis of data acquired on-line from a turning process using two differently coated indexable inserts has been investigated and the results presented. Based on the analysis carried out, it was possible to identify trends in the sensor signals as the tool insert wore. The determined characteristics showed that the sensor signals were affected by the different wear modes occurring simultaneously on the tool insert. The results indicated that the magnitudes of the static cutting forces were overwhelmingly dependent on the cutting conditions especially the DOC and feed-rate.

Overall, the result trend seem to suggest that the vertical components (z-direction) of both cutting forces and the vibration signatures were the most sensitive to tool wear, with nose wear being the most useful indicator of eminent tool failure. The cutting conditions invariable are a major factor affecting the process parameters. Their independence in the design of any TCMS can not therefore be neglected evident by variation in the sensitivity of the cutting forces (static and dynamic) as well as the vibration components to both tool wear and cutting conditions. It has also been possible to separate and identify changes in the sensor signals originating from changes in cutting conditions as opposed to those arising from changes in the wear on the cutting tool. The static force in this case was the most sensitive indicator of cutting condition changes such as DOC and feed-rate while the dynamic sensors were good at tracking changes in the sensors from accrued wear. Based on the analyses performed and interpretations of features on the presented graphs, selection of the sensor signals has been justified. The cutting conditions,

self-evidently would be incorporated into the input vector set for reasons already outlined, and used in part II of this paper as inputs to a multi-layer perceptron neural network paradigm, and its ability to distinguishing and classify tool state investigated.

Acknowledgements

The authors would like to thank the Research Support Unit at the University of Wolverhampton for providing the funds, facilities and support to carry out this work. The assistance and encouragement of Dr Nigel Leighton throughout the first author's postgraduate studies is gratefully acknowledged. Thanks to Maria Giovanna Lo Porto for painstakingly producing the graphs.

References

[1] D.E. Dimla Sr, Multivariate tool condition monitoring in a metal cutting operation using neural networks, Ph.D. thesis, School of Engineering, The University of Wolverhampton, 1998.
[2] M.C. Shaw, Metal Cutting Principles, chap. 4, Clarendon Press, Oxford, 1984, pp. 18-46.
[3] P.M. Lister, On-line measurement of tool wear, Ph.D. thesis, Manufacturing and Machine Tools Division, Department of Mechanical Engineering, UMIST, 1993.
[4] T.J. Ko, D.W. Cho, Cutting state monitoring in milling by a neural network, Int. J. Mach. Tools Manufact. 34 (5) (1994) 659–676.
[5] O. Masory, Detection of tool wear using multi-sensor readings defused by artificial neural network, Proc. SPIE—Int. Soc. Optical Engng 1469(2) (1991) 515–525.
[6] S. Purushothaman, Y.G. Srinivasa, A back-propagation algorithm applied to tool wear monitoring, Int. J. Mach. Tools Manufact. 34 (5) (1994) 625–631.
[7] I.N. Tansel, C. Mekdeci, C. McLaughlin, Detection of tool failure in end milling with wavelet transformations and neural networks, ASME PED Manufact. Sci. Engng 64 (1994) 369–374.
[8] I.N. Tansel, O. Rodriguez, C. Mekdeci, Detection of tool breakage in micro-drilling operation with RCE neural networks, ASME PED Engng Syst. Design Analysis 47 (1) (1992) 83–88.
[9] I.N. Tansel, A. Wagiman, A. Tziranis, Recognition of chatter with neural networks, Int. J. Mach. Tools Manufact. 31 (4) (1991) 539–552.
[10] S. Rangwala, D. Dornfeld, Integration of sensors via neural networks for detection of tool wear states, ASME PED 25 (1987) 109–120.
[11] S. Rangwala, D. Dornfeld, Sensor integration using neural networks for intelligent tool condition monitoring, Trans. ASME J. Engng Ind. 112 (3) (1990) 219–228.
[12] E.M. Trent, Metal Cutting, Butterworths, London, 1977.
[13] S.V. Karmathi, On-line tool wear estimation in turning through sensor data fusion and neural networks, Ph.D. thesis, Department of Industrial and Manufacturing Engineering, The Pennsylvania State University, 1994.
[14] D. Guinea, A. Ruiz, L.J. Barrios, Multi-sensor integration—an automatic feature selection and sate identification methodology for tool wear estimation, Computers in Industry 17 (1991) 121–130.
[15] G.S. Choi, Z.X. Wang, D.A. Dornfeld, K. Tsujino, Development of an intelligent on-line tool wear monitoring system for turning operations, Proc. USA–Japan Symposium on Flexible Automation, A Pacific Rim Conference ISCIE, Kyoto, Japan, 1990, pp. 683–690.
[16] G. Byrne, D. Dornfeld, I. Inasaki, G. Ketteler, W. König, R. Teti, Tool Condition Monitoring Systems (TCMS)—the state of research and industrial application, Annals of CIRP 44 (2) (1995) 541–567.
[17] S.E. Oraby, D.R. Hayhurst, Development of models for tool wear force relationships in metal cutting, Int. J. Mach. Tools Manufact. 33 (2) (1991) 125–138.
[18] L.I. Burke, Automated identification of tool wear states in machining processes: an application of self-organising

neural networks, Ph.D. thesis, Department of Industrial Engineering and Operations Research, UC at Berkeley, 1989.
[19] AB Sandvik Coromant Metal Working Products Catalogue-Turning Tools, 1995.
[20] R.L. Hatschek, Turning with inserts, American Machinist (1978) 101–116.
[21] T. Shi, S. Ramalingam, Real-time flank wear sensing, ASME Winter Annual Meeting PED 43 (1990) 157–170.
[22] K.S. Lee, L.C. Lee, S.C. Teo, On-line tool wear monitoring using a PC, J. Material Process Technology 29 (1992) 3–13.
[23] L.C. Lee, K.S. Lee, C.S. Gan, On the correlation between dynamic cutting force and tool wear, Int. J. Mach. Tools Manufact. 29 (3) (1989) 295–303.
[24] G. Warnecke, A. Jenewein, A. Reinfelder, Tool monitoring based on process identification, monitoring and control for manufacturing processes, ASME Winter Annual Meeting, Dallas, TX, 1990, pp. 43–55.